INŽENÝRSKÁ MECHANIKA 2005
NÁRODNÍ KONFERENCE
s mezinárodní účastí
Svratka, Česká republika, 9. - 12. května 2005

NUMERICAL SOLUTION OF THE COMPRESSIBLE TURBULENT FLOW THROUGH THE GAP CAUSED BY THE INCORRECT CONTACT OF SCREW SURFACES

J. Vimmr*, J. Švígler*

Summary: *The paper deals with the numerical simulation of a turbulent compressible fluid flow through the two-dimensional model of a gap caused by the incorrect contact of screw surfaces. The incorrect contact of screw surfaces considered in this paper is caused by a large parallel displacement of the axis of one of the surfaces. Numerical solution of the nonlinear conservative system of the Favre-averaged Navier-Stokes equations is obtained by means of the cell-centred finite volume formulation of the explicit two-step TVD MacCormack scheme proposed by Causon on a structured quadrilateral grid. To simulate the turbulence effects the algebraic Baldwin-Lomax turbulence model is implemented into the own developed numerical code.*

1. Introduction

The most important part of the screw machines, i.e. screw compressors or expanders that create in combination with compressors the screw engines, is the work space, where the fluid is compressed. It has a complicated geometry which changes during the motion of two rotors. The processes, which take place in the work space and in the gaps on its boundaries, have a great influence on the performance of the screw compressor, especially with regard to its internal efficiency. The knowledge of the processes in the gaps on the boundaries of the work space enables to make reasonable estimates for the mass flow rate and to define the loss of the medium. Therefore it is necessary to investigate the details of the leakage flow.

In (Vimmr & Švígler, 2004), the laminar computation of the leakage flow through the two-dimensional model of the gap caused by the incorrect contact of screw surfaces for the pressure ratio $p_{inlet}/p_{outlet} = 2$ was presented. It was assumed that the leakage flow in this gap of 0.1 mm height, which represents a very narrow channel where the reference Reynolds number is $Re_\infty = 3900$, could be laminar. But from the obtained results it seems that this assumption of the laminar flow computation is not exactly correct. Therefore the aim of this paper is to include the effects of turbulence in a flow field and to perform the turbulent flow computation through this gap.

* Ing. Jan Vimmr, Ph.D., Doc. Ing. Jaromír Švígler, CSc.: Západočeská univerzita v Plzni, Fakulta aplikovaných věd, Katedra mechaniky; Univerzitní 22; 306 14 Plzeň; tel.: +420.377 632 314, fax: +420.377 632 302; e-mail: jvimmr@kme.zcu.cz

2. Formulation of the problem

The incorrect contact of screw surfaces σ_2 and σ_3 caused by a large parallel displacement $\Delta \boldsymbol{r}_{O_3} = [\Delta x_{O_3}, \Delta y_{O_3}, 0]$ of axis o_3 of the surface σ_3 was solved and presented in (Vimmr & Švígler, 2004). The surface σ_3 is displaced in a new position σ_3^{Δ}, Fig. 1. The first contact of surfaces σ_2 and σ_3^{Δ} takes place in the cross section τ, which is defined by $\varphi_3^P = \min\{{}^j\varphi_3^P\}$, $j \in (1, m)$, where φ_3^P is the angle of rotation of the surface σ_3^{Δ} towards the contact position of surfaces σ_3^{Δ} and σ_2. For the numerical solution of the incorrect contact of screw surfaces the following basic values were considered: the axis distance $a_w = 100$ mm, gear ratio $i_{32} = \frac{3}{2}$, the helix angle on the rolling cylinder of both rotors $\gamma = 45°$, radius $r_k = 125$ mm of the circle k_3, displacements $\Delta x_{O_3} = 0.1$ mm and $\Delta y_{O_3} = 0.1$ mm of axis o_3. The incorrect contact of surfaces σ_2 and σ_3^{Δ} is demonstrated in Fig. 2, where CH_{32} is the contact point.

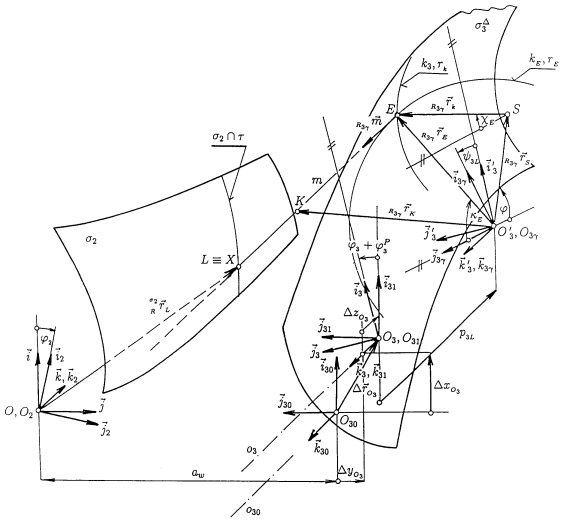

Fig. 1 Creating of the incorrect contact of surfaces σ_2 a σ_3.

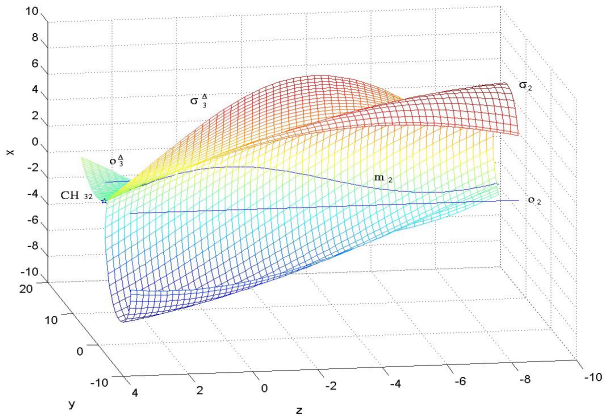

Fig. 2 The incorrect contact of surfaces σ_2 a σ_3^{Δ}.

This situation should be well observed in the cross section for $p_{3L} = -68$ mm of surfaces σ_2 and σ_3^{Δ} with the incorrect contact, Fig. 3, where the detail of the gap caused by this incorrect contact of screw surfaces is shown on the right. The contact of surfaces in the contact point CH_{32} takes place in the cross section for $p_{3L} = 34{,}04$ mm.

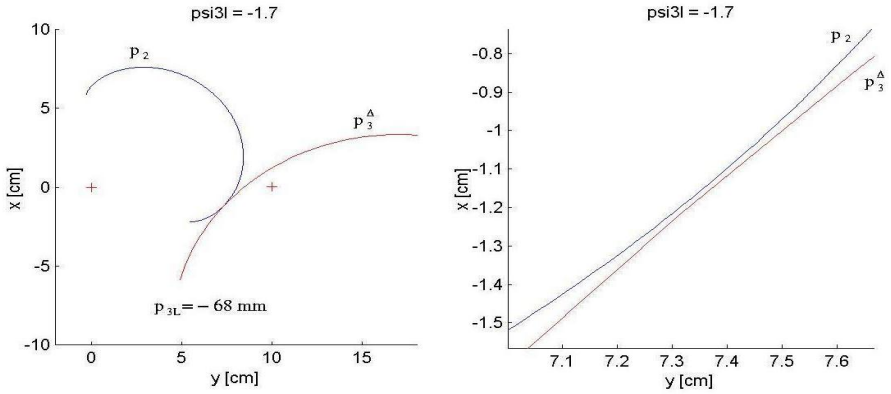

Fig. 3 The cross section for $p_{3L} = -68$ mm of surfaces σ_2 and σ_3^{Δ} with the incorrect contact.

The computational model of the gap caused by the incorrect contact of screw surfaces in the cross section for $p_{3L} = -68$ mm was created in (Vimmr & Švígler, 2004), where the profile p_3^{Δ} of the surface σ_3^{Δ} is considered as the circle $k_3(S, r_k)$, Fig. 1, and the profile p_2 of the surface σ_2 is replaced by an osculating circle. The profile p_2 creates the upper curve of the planar computational model of the gap, Fig. 3. This computational model of the gap caused by the incorrect contact of screw surfaces in the cross section for $p_{3L} = -68$ mm can be modelled by a two-dimensional bounded domain $\Omega \subset \mathbb{R}^2$, occupied by a calorically perfect gas, with the Lipschitz boundary $\partial\Omega = \partial\Omega_I \cup \partial\Omega_O \cup \partial\Omega_W$, where $\partial\Omega_I$ is the inlet and $\partial\Omega_O$ the outlet section of the computational domain Ω and $\partial\Omega_W = \partial\Omega_W^{p_2} \cup \partial\Omega_W^{p_3^{\Delta}}$ are impermeable walls of the computation domain corresponding to the osculating circle p_2 and to the profile p_3^{Δ}.

In (Vimmr & Švígler, 2004), the laminar computation of the compressible fluid flow through this gap for the pressure ratio $p_{inlet}/p_{outlet} = 2$ was presented. It was assumed that the leakage flow in this gap of 0.1 mm height, which represents a very narrow channel where the reference Reynolds number $Re_\infty = 3900$, could be laminar. But from the obtained results, (Vimmr & Švígler, 2004), it seems that this assumption of the laminar flow computation is not exactly correct. Therefore it is necessary to include the effects of turbulence in a flow field and to perform the turbulent flow computation through this gap.

3. Mathematical model of a turbulent compressible fluid flow

Let $\Omega \subset \mathbb{R}^2$ be a computational domain with a boundary $\partial\Omega$ and $(0, \mathcal{T})$ a time interval. In the laminar case, the motion of a compressible, viscous, heat-conducting, Newtonian fluid is described by the well-known nonlinear conservative system of the Navier-Stokes (NS) equations derived from the integral form of the conservation laws for mass, momentum and total energy in Eulerian description, (Vimmr, November 2003). In order to obtain the governing conservation equations for turbulent flows, it is convenient to replace the instantaneous quantities in the system of the NS equations by their mean and their fluctuating values.

If $\Phi(\boldsymbol{y}, t)$ is any time dependent flow variable, two different types of averaging of $\Phi(\boldsymbol{y}, t)$ can be defined:

- conventional time averaging introduced by Reynolds in which the instantaneous flow variable $\Phi(\boldsymbol{y}, t)$ is expressed as the sum of a mean $\overline{\Phi}(\boldsymbol{y}, t)$ and a fluctuating part $\Phi'(\boldsymbol{y}, t)$, so that

$$\Phi(\boldsymbol{y}, t) = \overline{\Phi}(\boldsymbol{y}, t) + \Phi'(\boldsymbol{y}, t)\,, \tag{1}$$

$$\overline{\Phi}(\boldsymbol{y}, t) = \frac{1}{\Delta t}\int_{t_0}^{t_0+\Delta t} \Phi(\boldsymbol{y}, t)\, dt\,. \tag{2}$$

- mass-weighted time averaging suggested by Favre in which the instantaneous flow variable $\Phi(\boldsymbol{y}, t)$ is decomposed into the mass-averaged part $\widetilde{\Phi}(\boldsymbol{y}, t)$ and a fluctuating part $\Phi''(\boldsymbol{y}, t)$, wherefore

$$\Phi(\boldsymbol{y}, t) = \widetilde{\Phi}(\boldsymbol{y}, t) + \Phi''(\boldsymbol{y}, t)\,, \tag{3}$$

$$\widetilde{\Phi}(\boldsymbol{y}, t) = \frac{\overline{\varrho\Phi}}{\overline{\varrho}}\,, \tag{4}$$

where the bar denotes conventional time averaging. Note the important differences between the two averaging procedures. In the conventional time averaging, $\overline{\Phi'} = 0$ and $\overline{\varrho\Phi'} \neq 0$; in the mass-weighted averaging, $\overline{\Phi''} \neq 0$ and $\overline{\varrho\Phi''} = 0$.

Introducing a conventional time average decomposition (1) of density ϱ and static pressure p and a mass-weighted time average decomposition (3) of the velocity vector v_j, total energy E per unit volume and thermodynamic temperature T and performing the mass-averaging operations described precisely in (Vimmr, March 2003), we arrive at the nonlinear system of the Favre-averaged Navier-Stokes (FANS) equations written in nondimensional conservative form

$$\frac{\partial \boldsymbol{w}}{\partial t} + \sum_{j=1}^{2} \frac{\partial \boldsymbol{\mathcal{F}}_j^I(\boldsymbol{w})}{\partial y_j} = \frac{1}{Re_\infty} \sum_{j=1}^{2} \frac{\partial \boldsymbol{\mathcal{F}}_j^V(\boldsymbol{w})}{\partial y_j} \qquad \text{in} \quad \Omega \times (0, \mathcal{T}) \,. \tag{5}$$

The column vector $\boldsymbol{w}$ of conservative variables and the vectors $\boldsymbol{\mathcal{F}}_j^I(\boldsymbol{w})$ of inviscid and $\boldsymbol{\mathcal{F}}_j^V(\boldsymbol{w})$ of viscous fluxes are given by

$$\boldsymbol{w} = \left(\overline{\varrho},\ \overline{\varrho}\,\widetilde{v_1},\ \overline{\varrho}\,\widetilde{v_2},\ \widetilde{E}\right)^T , \tag{6}$$

$$\boldsymbol{\mathcal{F}}_j^I(\boldsymbol{w}) = \left(\overline{\varrho}\,\widetilde{v_j},\ \overline{\varrho}\,\widetilde{v_1}\widetilde{v_j} + \overline{p}\,\delta_{1j},\ \overline{\varrho}\,\widetilde{v_2}\widetilde{v_j} + \overline{p}\,\delta_{2j},\ (\widetilde{E} + \overline{p})\widetilde{v_j}\right)^T , \qquad j = 1, 2 \,, \tag{7}$$

$$\boldsymbol{\mathcal{F}}_j^V(\boldsymbol{w}) = (0,\ \widetilde{\tau_{1j}},\ \widetilde{\tau_{2j}},\ \widetilde{\tau_{1j}}\widetilde{v_1} + \widetilde{\tau_{2j}}\widetilde{v_2} - \widetilde{q_j})^T , \qquad j = 1, 2 \,, \tag{8}$$

where δ_{ij} is Kronecker delta and

$$\widetilde{\tau_{ij}} = \widetilde{\tau_{ij}}^{lam} + \widetilde{\tau_{ij}}^{turb} \equiv (\eta + \eta_t) \left(\frac{\partial \widetilde{v_i}}{\partial y_j} + \frac{\partial \widetilde{v_j}}{\partial y_i} - \frac{2}{3}\delta_{ij} \frac{\partial \widetilde{v_k}}{\partial y_k} \right) , \qquad i, j = 1, 2 \,, \tag{9}$$

$$\widetilde{q_j} = \widetilde{q_j}^{lam} + \widetilde{q_j}^{turb} \equiv -\frac{\kappa}{\kappa - 1} \left(\frac{\eta}{Pr} + \frac{\eta_t}{Pr_t} \right) \frac{\partial}{\partial y_j} \left(\frac{\overline{p}}{\overline{\varrho}} \right) , \qquad j = 1, 2 \,. \tag{10}$$

Since the fluctuating component of the molecular viscosity η is usually small, it has been neglected. The external volume forces are not considered in our case and additional closure approximations have been postulated. The turbulent shear stresses $\widetilde{\tau_{ij}}^{turb} \equiv -\overline{\varrho v_i'' v_j''}$ in relations (9) are modelled using the Boussinesq approximation, (Wilcox, 1993), where the concept of a turbulent (or eddy) viscosity η_t is introduced. The turbulent heat flux vectors $\widetilde{q_j}^{turb} \equiv c_p\, \overline{\varrho T v_j''}$ in (10) are modelled using a gradient approximation written in a form such as to resemble the laminar heat flux vectors. For this purpose, a turbulent Prandtl number Pr_t is defined. A constant value for Pr_t equal to 0.9 is often used for wall bounded flows.

Assuming a calorically perfect gas, the static pressure is given by the equation of state

$$\overline{p} = \overline{\varrho}\, r\, \widetilde{T} = (\kappa - 1)\, \overline{\varrho}\, c_v\, \widetilde{T} \equiv (\kappa - 1) \left(\widetilde{E} - \frac{1}{2}\, \overline{\varrho}\, \widetilde{v_j} \widetilde{v_j} \right) , \tag{11}$$

where $r = c_p - c_v$ is the gas constant per unit mass, c_p and c_v are the specific heats at constant pressure and volume, respectively and κ is Poisson´s constant. The laminar Prandtl number $Pr = c_p \eta / k$ is taken to be 0.72 for a calorically perfect gas, where k is thermal conductivity and $Re_\infty = \varrho_{ref} u_{ref} l_{ref} / \eta_{ref}$ is the reference Reynolds number. It rests to determine the turbulent viscosity η_t.

For computation of the turbulent viscosity η_t an algebraic Baldwin-Lomax turbulence model is considered. The description of algebraic turbulence models can be found for example in (Příhoda, 1990; Wilcox, 1993). The Baldwin-Lomax model is a two-layer turbulence model, based on the mixing-length hypothesis, which is formulated for use in computations where boundary-layer properties such as the boundary-layer thickness δ, the kinetic displacement thickness δ_v^* and the boundary-layer edge velocity u_e are difficult to determine. This situation often arises in numerical simulation of separated flows. The turbulent viscosity η_t is given by using a two-layer approach,

$$\eta_t = \begin{cases} \eta_{t_i} & \text{if} \quad y \le y_m \quad \ldots \text{ the inner layer} \\ \eta_{t_o} & \text{if} \quad y > y_m \quad \ldots \text{ the outer layer} \end{cases} , \tag{12}$$

where y is the normal distance from the wall and y_m is the smallest value of y for which $\eta_{t_i} = \eta_{t_o}$. For the wake region, the inner layer is not defined so we have $\eta_t = \eta_{t_o}$.

In the inner layer, η_{t_i}, is computed as follows

$$\eta_{t_i} = \overline{\varrho}\, l_{mix}^2 \, |\omega| \,, \tag{13}$$

$$l_{mix} = \gamma \, y \, F_{_D} \,, \qquad F_{_D} = 1 - e^{-y^+/A^+}, \qquad \omega = \frac{\partial \widetilde{u}}{\partial y} - \frac{\partial \widetilde{v}}{\partial x} \,, \tag{14}$$

where γ is the von Karman constant, the mixing length l_{mix} is determined by the van Driest function $F_{_D}$ and ω is the vorticity. The nondimensional space coordinate y^+, normal to the wall, can be written as

$$y^+ = \frac{y}{\eta_w} \sqrt{\overline{\varrho_w} \, |\widetilde{\tau_w}|} \,, \qquad \widetilde{\tau_w} = \eta_w \left. \frac{\partial \widetilde{u}}{\partial y} \right|_{y=0} , \tag{15}$$

where $\widetilde{\tau_w}$ is the wall shear stress in the direction of the flow and the subscript w indicates the wall quantities.

In the outer layer, η_{t_o}, is given by

$$\eta_{t_o} = \overline{\varrho}\, \alpha \, C_{cp} \, F_{wake} \, F_{kleb} \,, \tag{16}$$

$$F_{wake} = \min \left(y_{\max} \, G_{\max} \,, \, C_{wake} \, y_{\max} \, \frac{(\Delta V)^2}{G_{\max}} \right) , \quad G_{\max} = \max_y \left(y \, |\omega| \, F_{_D} \right) , \tag{17}$$

where $y_{\max}$ is the value of y where $G_{\max}$ occurs, $G(y_{\max}) = G_{\max}$, and ΔV is the difference between the absolute values of the maximum and minimum velocities within the viscous region for $x = const$. For wall bounded flows, the minimum velocity occurs at the wall where the velocity is zero, then $\Delta V = (\widetilde{u}^{\,2} + \widetilde{v}^{\,2})^{1/2}_{\max}$. For shear layer flows, ΔV is defined as the difference between the maximum velocity in the layer and the velocity at the $y_{\max}$ location, that is, $\Delta V = (\widetilde{u}^{\,2} + \widetilde{v}^{\,2})^{1/2}_{\max} - (\widetilde{u}^{\,2} + \widetilde{v}^{\,2})^{1/2}_{y_{\max}}$ for $x = const$. The Klebanoff's intermittency factor F_{kleb} is given by

$$F_{kleb} = \left[1 + 5.5 \left(C_{kleb} \, \frac{y}{y_{\max}} \right)^6 \right]^{-1} . \tag{18}$$

The model constants are: $\gamma = 0.4$, $A^+ = 26$, $\alpha = 0.0168$, $C_{cp} = 1.6$, $C_{wake} = 0.25$, $C_{kleb} = 0.3$.

Finally, the turbulent viscosity distribution across the boundary layer is determined as

$$\eta_t = \min(\eta_{t_i},\, \eta_{t_o}) \tag{19}$$

and $\eta_{t_i} := \infty$ for the wake. To initiate the computations, a transition location x_{tr} is specified, and the initial value of the turbulent viscosity is set equal to zero everywhere within the computational domain. Subsequently, in regions where $x > x_{tr}$, the turbulent viscosity is computed from (19) and updated after each time step.

4. Numerical method

To solve the nonlinear conservative system of the FANS equations (5), the same numerical method as for the laminar case is used, (Vimmr, November 2003), only the viscous coefficient is replaced by the sum of the molecular and turbulent viscosities. The turbulent viscosity η_t is computed by using the algebraic Baldwin-Lomax turbulence model. The advantage of the algebraic models is that no additional equations have to be solved. The Baldwin-Lomax model is mathematically simple and its implementation into the own developed numerical code for the laminar flow computation is easy.

For the discretization of the system of the FANS equations (5) the cell-centred finite volume (FV) method on a structured quadrilateral grid, (Vimmr, November 2003), is used. Time integration of the inviscid part of the system (5) is performed by using the FV formulation of the explicit two-step TVD MacCormack scheme proposed by Causon, (Causon, 1989). The approximations of the viscous part of the system (5) are added to the predictor and corrector steps of the MacCormack scheme

$$\boldsymbol{w}_{ij}^{n+\frac{1}{2}} = \boldsymbol{w}_{ij}^{n} - \frac{\Delta t}{|\Omega_{ij}|}\sum_{m=1}^{4}\left(\boldsymbol{f}_m^n\, S_m^x + \boldsymbol{g}_m^n\, S_m^y\right) + \frac{\Delta t}{|\Omega_{ij}|}\, Visc(\boldsymbol{w}_{ij}^n)\,, \tag{20}$$

$$\overline{\boldsymbol{w}_{ij}^{n+1}} = \frac{1}{2}\left\{\boldsymbol{w}_{ij}^{n} + \boldsymbol{w}_{ij}^{n+\frac{1}{2}} - \frac{\Delta t}{|\Omega_{ij}|}\sum_{m=1}^{4}\left(\boldsymbol{f}_m^{n+\frac{1}{2}} S_m^x + \boldsymbol{g}_m^{n+\frac{1}{2}} S_m^y\right)\right\} + \frac{1}{2}\,\frac{\Delta t}{|\Omega_{ij}|}\, Visc(\boldsymbol{w}_{ij}^{n+\frac{1}{2}})\,, \tag{21}$$

$${}^{(TVD)}\boldsymbol{w}_{ij}^{n+1} = \overline{\boldsymbol{w}_{ij}^{n+1}} + d\boldsymbol{w}_{ij}^{1n} + d\boldsymbol{w}_{ij}^{2n}\,, \tag{22}$$

where ${}^{(TVD)}\boldsymbol{w}_{ij}^{n+1}$ is the corrected numerical solution at time t_{n+1} and $|\Omega_{ij}|$ denotes the face area of the finite volume Ω_{ij}. The Cartesian components $\boldsymbol{f}_m$ and $\boldsymbol{g}_m$ of the inviscid numerical fluxes $\boldsymbol{\mathcal{F}}_m^I$ through the edges $\Gamma_{ij}^m,\ m = 1, \ldots, 4$, of the cell Ω_{ij} at time t_n are evaluated as

$$\begin{aligned}
&\boldsymbol{f}_1^n = \boldsymbol{f}(\boldsymbol{w}_{i+1j}^n)\,, \qquad \boldsymbol{f}_2^n = \boldsymbol{f}(\boldsymbol{w}_{ij+1}^n)\,, \qquad \boldsymbol{f}_3^n \equiv \boldsymbol{f}_4^n = \boldsymbol{f}(\boldsymbol{w}_{ij}^n)\,,\\
&\boldsymbol{g}_1^n = \boldsymbol{g}(\boldsymbol{w}_{i+1j}^n)\,, \qquad \boldsymbol{g}_2^n = \boldsymbol{g}(\boldsymbol{w}_{ij+1}^n)\,, \qquad \boldsymbol{g}_3^n \equiv \boldsymbol{g}_4^n = \boldsymbol{g}(\boldsymbol{w}_{ij}^n)
\end{aligned}$$

and at time $t_{n+\frac{1}{2}}$ as

$$\begin{aligned}
&\boldsymbol{f}_1^{n+\frac{1}{2}} \equiv \boldsymbol{f}_2^{n+\frac{1}{2}} = \boldsymbol{f}(\boldsymbol{w}_{ij}^{n+\frac{1}{2}})\,, \qquad \boldsymbol{f}_3^{n+\frac{1}{2}} = \boldsymbol{f}(\boldsymbol{w}_{i-1j}^{n+\frac{1}{2}})\,, \qquad \boldsymbol{f}_4^{n+\frac{1}{2}} = \boldsymbol{f}(\boldsymbol{w}_{ij-1}^{n+\frac{1}{2}})\,,\\
&\boldsymbol{g}_1^{n+\frac{1}{2}} \equiv \boldsymbol{g}_2^{n+\frac{1}{2}} = \boldsymbol{g}(\boldsymbol{w}_{ij}^{n+\frac{1}{2}})\,, \qquad \boldsymbol{g}_3^{n+\frac{1}{2}} = \boldsymbol{g}(\boldsymbol{w}_{i-1j}^{n+\frac{1}{2}})\,, \qquad \boldsymbol{g}_4^{n+\frac{1}{2}} = \boldsymbol{g}(\boldsymbol{w}_{ij-1}^{n+\frac{1}{2}})\,.
\end{aligned}$$

$\boldsymbol{S}_m = \left(S_m^x\,,\ S_m^y\right)^T$ are cell side normal vectors to the edges Γ_{ij}^m, where we designate: $\boldsymbol{S}_1 = \boldsymbol{S}_{i+\frac{1}{2}j}$, $\boldsymbol{S}_2 = \boldsymbol{S}_{ij+\frac{1}{2}}$, $\boldsymbol{S}_3 = \boldsymbol{S}_{i-\frac{1}{2}j}$ and $\boldsymbol{S}_4 = \boldsymbol{S}_{ij-\frac{1}{2}}$. The viscous terms $Visc(\boldsymbol{w}_{ij})$ in (20) and (21) are

approximated by using a FV version with central differences, see (Vimmr, November 2003) for details. The added one-dimensional TVD-type viscosity terms $d\boldsymbol{w}_{ij}^{1n}$ and $d\boldsymbol{w}_{ij}^{2n}$ in the directions of the change of index i and j respectively, are defined by Causon, (Causon, 1989).

5. Numerical results

For the turbulent computation of the compressible viscous fluid flow through the two-dimensional model of the gap caused by the incorrect contact of screw surfaces the same computational grid with 190×64 quadrilateral cells as for the laminar flow computation presented in (Vimmr & Švígler, 2004) is used and the same reference Reynolds number $Re_\infty = 3900$ and boundary conditions are considered. At the inlet $\partial\Omega_I$, the stagnation pressure $\overline{p_{01}} = 1$, the stagnation temperature $\widetilde{T_{01}} = 1$, the inlet angle α_1, $\frac{\partial \widetilde{T}}{\partial \boldsymbol{n}} = 0$ and $\sum_{j=1}^{2} \widetilde{\tau^{ij}} n_j = 0$, $i = 1, 2$ are prescribed. At the outlet $\partial\Omega_O$, the static pressure $\overline{p_2} = 0.5$, $\frac{\partial \widetilde{T}}{\partial \boldsymbol{n}} = 0$ and $\sum_{j=1}^{2} \widetilde{\tau^{ij}} n_j = 0$, $i = 1, 2$ are kept. On the solid walls $\partial\Omega_W^{p_2}$ and $\partial\Omega_W^{p_3^\Delta}$, the boundary conditions $\widetilde{u} = 0$, $\widetilde{v} = 0$ and $\frac{\partial \widetilde{T}}{\partial \boldsymbol{n}} = 0$ are satisfied. $\boldsymbol{n}$ is the outward unit normal vector to the boundary.

Fig. 4 displays the isolines of the Mach number in the gap plotted with $\Delta M = 0.02$. The separation of the flow is simulated from the position where the height of the gap enlarges. The flow is transonic $M_{max} \approx 1.6$ and it seems to be stationary in contrast to the numerical results obtained by using the laminar flow computation presented in (Vimmr & Švígler, 2004), where the flow is non-stationary, see Fig. 5, in which the isolines of the Mach number in the gap plotted with $\Delta M = 0.02$ at time $t = 2.798 \cdot 10^{-4}$ s are shown. The changes in the shape of the wake are observed in the laminar case and the maximum values of the Mach number change from $M_{max} \approx 1.1$ to $M_{max} \approx 1.4$.

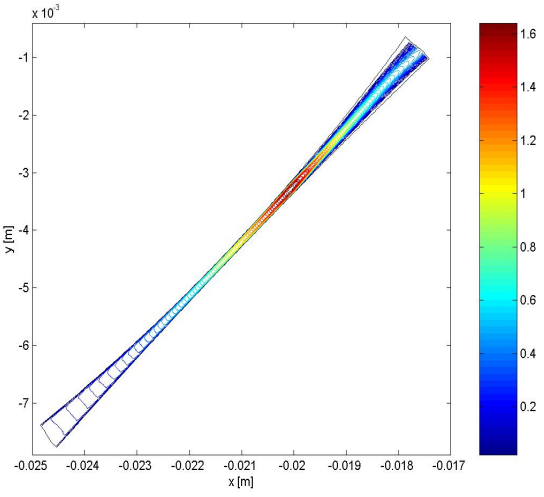

Fig. 4 Isolines of the Mach number in the gap (turbulent flow computation).

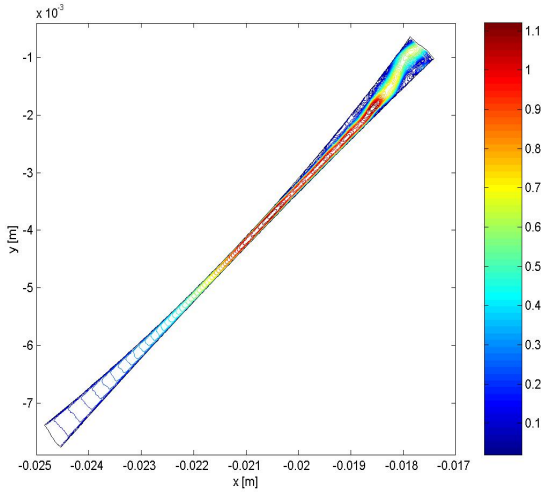

Fig. 5 Isolines of the Mach number in the gap (laminar flow computation).

The velocity magnitude distribution and the isolines of the static pressure in the two-dimensional model of the gap caused by the incorrect contact of screw surfaces are shown in Fig. 6 and Fig. 7, respectively.

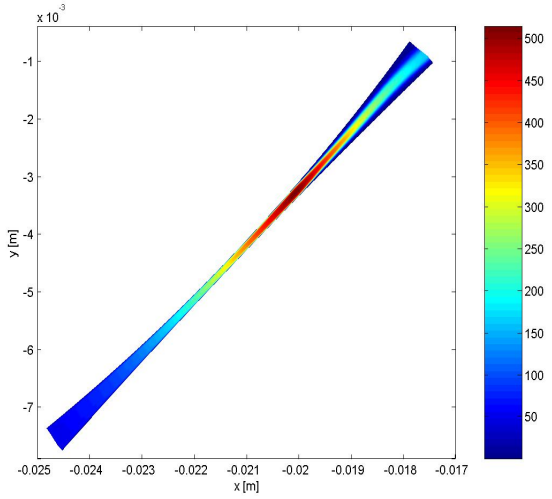

Fig. 6 Velocity magnitude distribution in [m/s] (turbulent flow computation).

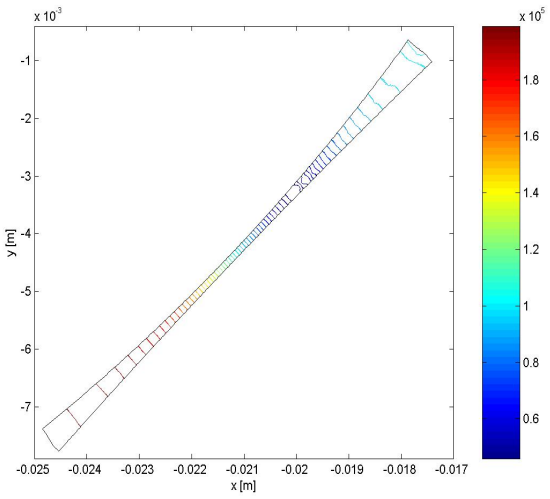

Fig. 7 Isolines of the static pressure in [Pa] (turbulent flow computation).

The static pressure distribution along a middle streamline in this gap for the turbulent flow computation is visualized in Fig. 8. It can be seen that the presribed pressure ratio $p_{inlet}/p_{outlet} = 2$ is satisfied. Fig. 9 displays the static pressure distribution along a middle streamline in the gap for the laminar flow computation at time $t = 2.798 \cdot 10^{-4}$ s.

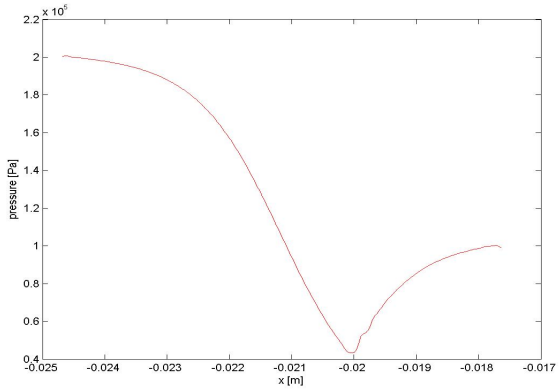

Fig. 8 Static pressure distribution in the gap (turbulent flow computation).

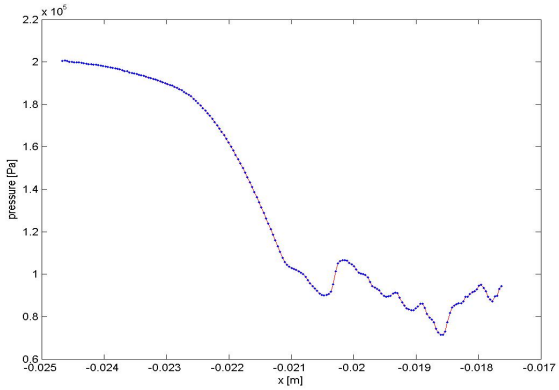

Fig. 9 Static pressure distribution in the gap (laminar flow computation).

The value $\dot{m} = 0.0445$ kg/ms of the mass flow rate per unit width for the turbulent flow computation through the gap caused by the incorrect contact of screw surfaces is determined. For the sake of completeness, the mass flow rates per unit width in dependence on the time for the laminar flow computation through this gap presented in (Vimmr & Švígler, 2004) are shown in Fig. 10.

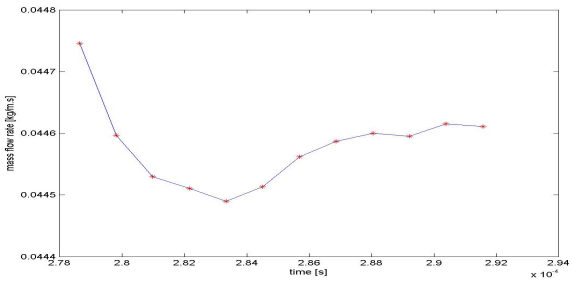

Fig. 10 Mass flow rates per unit width (laminar flow computation).

6. Conclusions

Numerical method for the computation of a turbulent compressible fluid flow through the two-dimensional model of the gap caused by the incorrect contact of screw surfaces based on the algebraic Baldwin-Lomax turbulence model was presented in this paper.

As a conclusion of our numerical testing we can deduce that the leakage flow through this gap for the pressure ratio $p_{inlet}/p_{outlet} = 2$ is transonic but without shock waves which are characteristic for transonic or supersonic flows. This is probably result of the very narrow gap. The turbulent flow computation gives the stationary results and converges better than the laminar flow computation that gives non-stationary results. The value of the mass flow rate per unit width for the turbulent flow computation through the gap caused by the incorrect contact of screw surfaces was determined.

7. Acknowledgements

This work was supported by the grant *GA ČR 101/03/P090* of the Grant Agency of the Czech Republic and by the research project *MSM 4977751303* of the Ministry of Education, Youth and Sports of the Czech Republic to which we express our grateful thanks.

8. References

Causon, D. M. (1989) High Resolution Finite Volume Schemes and Computational Aerodynamics, in: *Nonlinear Hyperbolic Equations - Theory, Computation Methods and Applications, Vol. 24 of Notes on Numerical Fluid Mechanics*, Vieweg, Braunschweig, pp. 63–74.

Příhoda, J. (1990) *Algebraické modely turbulence a jejich použití při řešení středovaných Navier-Stokesových rovnic*. Výzkumná zpráva Z–1153/90, Ústav termomechaniky ČSAV, Praha.

Vimmr, J. (March 2003) Introduction to the mathematical modelling of turbulent compressible fluid flow. *Zeszyty naukowe Katedry Mechaniki Stosowanej*, zeszyt nr. 21, pp. 207-212.

Vimmr, J. (November 2003) A treatise on numerical computation of non-stationary laminar compressible flow, in: *Proc. 19th conference with international participation Computational Mechanics 2003* (J. Vimmr ed.), University of West Bohemia in Pilsen, Hrad Nečtiny, pp. 483-494.

Vimmr, J. & Švígler, J. (2004) Analysis of the compressible viscous fluid flow through the gap caused by the incorrect contact of screw surfaces, in: *CD-ROM Proc. 10th national conference with international participation Engineering Mechanics 2004* (I. Zolotarev & A. Požívilová eds.), Inst. of Thermomechanics, Academy of Sciences of the Czech Republic in Prague, Svratka.

Wilcox, D. C. (1993) *Turbulence Modeling for CFD*. DCW Industries, La Cañada, California.